Molecular dynamics approach to vibrational energy relaxation: Quantum-classical versus purely classical nonequilibrium simulations

A. A. Neufeld, D. Schwarzer, J. Schroeder, and J. Troe

Citation: The Journal of Chemical Physics **119**, 2502 (2003); doi: 10.1063/1.1587125
View online: http://dx.doi.org/10.1063/1.1587125
View Table of Contents: http://scitation.aip.org/content/aip/journal/jcp/119/5?ver=pdfcov
Published by the AIP Publishing

Molecular dynamics approach to vibrational energy relaxation: Quantum-classical versus purely classical nonequilibrium simulations

A. A. Neufeld[a] and D. Schwarzer
Abteilung Spektroskopie und Photochemische Kinetik, Max-Planck-Institut für Biophysikalische Chemie, Am Fassberg, D-37077 Göttingen, Germany

J. Schroeder and J. Troe
Institut für Physikalische Chemie, Universität Göttingen, Tammanstrasse 6, D-37077 Göttingen, Germany D-37077 Göttingen, Germany

(Received 9 January 2003; accepted 6 May 2003)

We present an efficient method for the direct solution in the time domain of the equations of a novel recently proposed non-Markovian quantum-classical approximation, valid well beyond the applicability limits of both Redfield theory and Fermi's Golden Rule formula. The method is based on an *ab initio* molecular dynamics description of the classical bath and is suitable for applications to systems with a fairly large number of quantum levels. A simple model of the breathing sphere in a Lennard-Jones fluid was used to compare the results of the quantum-classical and purely classical treatments of vibrational energy relaxation. © *2003 American Institute of Physics.*
[DOI: 10.1063/1.1587125]

I. INTRODUCTION

Nonequilibrium molecular dynamics (NEMD) methods are widely used to simulate various phenomena in the condensed state, ranging from macroscopic[1,2] (transport phenomena) to microscopic processes[3–6] (energy transfer, relaxation processes, chemical reactions). NEMD techniques to a large extent rely on the validity of a classical description of the system under consideration. There are many situations, however, when quantum mechanical effects play an important role and a classical description is not justified. Examples are electron/nuclear transfer reactions (tunneling and/or highly nonadiabatic processes), dissociation of molecules (zero-point energy effects), or vibrational energy relaxation (VER). In the latter the splitting between energy levels often is comparable to the mean energy of the heat reservoir such that the discreteness of the energy spectrum comes into play, challenging the validity of a classical description, especially in highly anharmonic systems.

A quantum-classical approximation, where a small subset of states (internal states of reactants, reaction coordinates, etc.) is treated quantum-mechanically, while the other degrees of freedom are modeled by classical mechanics, seems to be a reasonable alternative both to a fully classical description and to a quantum-mechanical or semiclassical treatment of the entire system, which scale unfavorably with increasing number of degrees of freedom.

There exist a variety of quantum-classical approaches[7–32] suitable for describing a reacting systems interacting with a dissipative environment. They are, however, not equivalent to each other since any quantum-classical approximation introduces its own more or less uncontrolled approximation, and hence should be applied with care. In particular, the quantum-classical approaches based on wave function representations to modeling VER processes of solute molecules in liquids or dense gases seems to be doubtful, as the relaxed state of the molecule (canonical equilibrium) cannot be described by a wave function. On the other hand, to what extent an open quantum system interacting with thermal bath can be represented by an ensemble of pure states, still is an entirely open question, especially at finite temperature of the heat reservoir.

In contrast, approaches resulting in master equations for the reduced density matrix (RDM) of the quantum part of the system allow to incorporate canonical equilibrium and properly describe relaxation kinetics within certain applicability limits. A simple and widely used approach is the so-called Redfield theory,[19–22] which yields Markovian master equation, i.e., it completely neglects memory effects. However, it is valid at sufficiently long times $t \gg \tau_c$, where τ_c is the characteristic correlation time of the classical bath on the order of about 10 ps. Several non-Markovian theories[23–26] were suggested to overcome the restrictions of Redfield theory. These, however, require the solution of integrodifferential equations, which presents considerable numerical problems, such that up to now these approaches were not applied to the realistic multilevel systems.

Up to now the time-dependent perturbation theory in form of Fermi's Golden Rule is the most used approach[28–32] to calculate the rate of VER in liquids/supercritical fluids. Despite its simplicity (the VER rate appears to be proportional to the Fourier transform of the force–force correlation function at the given transition frequency), this approach assumes weak coupling and Markovian limits. Both conditions are quite restrictive, while the latter assumption proves to be questionable even for a heat reservoirs with a short correlation time, see Sec. VI.

Recently, we suggested a non-Markovian quantum-classical approximation[27] (NQCA) capable of describing the

[a]Electronic mail: aneufel@gwdg.de

evolution of open quantum system well beyond the applicability limits of Redfield theory. The approach utilizes the fast decay of cross-correlations between quantum subsystem and heat reservoir due to the energy dispersion of the degrees of freedom of the canonical bath. Despite the fact that this approach accounts for the arbitrary long memory of the surrounding medium, the resulting NQCA at times $t \gg \tau_b = \hbar/(\pi k_B T)$ is of differential form, and allows direct propagation of the quantum subsystem RDM in time without explicit construction or diagonalization of Liouville (super)operators. At room temperature $\tau_b = 8$ fs, which is considerably shorter than the correlation time τ_c of the classical bath. This also implies that a classical description of the bath degrees of freedom at times $t \lesssim \hbar/(k_B T)$ is not justified.

In the present article we develop an efficient MD-based method to solve the equations of our quantum-classical approximation directly in the time domain. The resulting NQCA-MD approach may be applied to fairly large quantum dynamical subsystems (QDS) consisting of up to several hundreds levels, using an *ab initio* description of the bath dynamics. The method is applied to VER of a one-dimensional harmonic oscillator (''breathing sphere'' model[32]) in a Lennard-Jones fluid. Although the ''breathing sphere'' model is somewhat oversimplified, it allows for a detailed comparison between classical (NEMD) and quantum-classical (NQCA-MD) treatments within the framework of the MD method. Note, that the method is not limited to the calculation of rates, it directly calculates the kinetics of VER, and is valid well beyond applicability limits of both Redfield theory and Fermi's Golden Rule formula. More realistic cases involving VER of diatomic (modeled by a Morse potential to include anharmonicity effects) and triatomic (energy redistribution between normal modes) molecules in a Lennard-Jones fluid, will be considered in subsequent articles.

II. QUANTUM-CLASSICAL APPROXIMATION

To write equations in a more compact form we set $\hbar = k_B = 1$, that is both interaction matrix elements and temperature are measured in rad/s. In these units $1\ \mathrm{K} = k_B/\hbar = 1.31 \times 10^{11}$ rad/s, and $1\ \mathrm{cm}^{-1} = 1.88 \times 10^{11}$ rad/s.

A quantum-classical approximation, as suggested in Ref. 27, requires the matrix elements of the system–bath coupling $\hat{W}(q)$ to satisfy the condition,

$$\frac{|W_{ik}(q)|}{\pi T} \ll 1, \tag{1}$$

where q denotes a generalized set of phase space coordinates. At times $t \gg \tau_b$, where

$$\tau_b = \frac{1}{\pi T} \tag{2}$$

is a characteristic lifetime of the system–bath cross-correlations caused by the energy dispersion of the bath degrees of freedom, the QCA is reduced to the following set of differential equations,[27]

$$\frac{d\sigma(t)}{dt} = -i[\hat{H}, \sigma(t)] - i \int [\hat{W}(q), \eta(q,t)] dq, \tag{3}$$

$$\frac{\partial \eta(q,t)}{\partial t} = -i[\hat{H}, \eta(q,t)] - i[\hat{W}(q), \sigma(t)] + [\hat{U}(q), \sigma(t)]_+ + \left[\hat{Y}(q), i[\hat{H}, \sigma(t)] + \frac{d\sigma(t)}{dt} \right]_+ + \mathcal{L}_q \eta(q,t), \tag{4}$$

where $\sigma(t)$ and $\eta(q,t)$ are the reduced density matrix of QDS and the auxiliary matrix, respectively, while $\mathcal{L}_q$ is linear functional operator defining motion of the system in phase space. Here,

$$\hat{U}(q) = i \sum_{l,m} a_{lm} \hat{P}^l \hat{W}(q) \hat{P}^m, \qquad \hat{Y}(q) = \sum_{l,m} b_{lm} \hat{P}^l \hat{W}(q) \hat{P}^m, \tag{5}$$

where

$$a_{lm} = \tanh\left(\frac{\omega_{lm}}{2T} \right), \quad b_{lm} = \frac{1}{2T} \frac{1}{\cosh^2\left(\frac{\omega_{lm}}{2T} \right)}, \tag{6}$$

and $\hat{P}^n$ are the projector operators on the eigenstates of the QDS Hamiltonian,

$$\hat{P}^n = |n\rangle\langle n|, \quad \hat{H}|n\rangle = E_n|n\rangle, \quad \omega_{lm} \equiv E_l - E_m. \tag{7}$$

The initial conditions for Eqs. (3) and (4) are of the form,

$$\sigma(t=0) = \sigma_0, \quad \eta(q, t=0) = [\hat{Y}(q), \sigma_0]_+, \tag{8}$$

where nonzero initial conditions for the auxiliary matrix account for correlations created during the short-time ($t \lesssim \tau_b$) evolution of the QDS, see Ref. 27 for more details.

The practical application of the quantum-classical approximation in form of Eqs. (3)–(7) to realistic multilevel QDSs is rather complicated. First, information about the linear functional operator $\mathcal{L}_q$ defining the motion in phase space is hardly available for nonmodel systems. Second, the solution of the partial differential equation (4) for the auxiliary matrix requires additional grids over phase space coordinates, which is prohibitively expensive for multilevel QDSs. However, the use of MD methods to simulate bath dynamics allows to overcome these difficulties. In this case integration over phase space coordinates is replaced by the MD average of the form,

$$\frac{d\sigma(t)}{dt} = -i[\hat{H}, \sigma(t)] - \lim_{N \to \infty} \frac{1}{N} \sum_{k=1}^{N} i[\hat{W}(q_k(t)), \eta_k(t)], \tag{9}$$

$$\frac{d\eta_k(t)}{dt} = -i[\hat{H}, \eta_k(t)] - i[\hat{W}(q_k(t)), \sigma(t)] + [\hat{U}(q_k(t)), \sigma(t)]_+ + \left[\hat{Y}(q_k(t)), i[\hat{H}, \sigma(t)] + \frac{d\sigma(t)}{dt} \right]_+, \tag{10}$$

where N in practice is a large number of MD trajectories sufficient to explore the phase space, while the system–bath interaction parametrically depends on time along a given MD trajectory. The proof of this statement is given below for the high temperature limit ($T\to\infty$), which is chosen as formulas appear in a more compact form. Its generalization to finite temperatures presents no difficulties.

The formal solution of Eq. (10) takes the form [$T\to\infty$, $\hat{U}(q)\to 0$, $\hat{Y}(q)\to 0$]

$$\eta_k(t) = -i\int_0^t e^{-i\hat{H}(t-\tau)}[\hat{W}(q_k(\tau)),\sigma(\tau)]e^{i\hat{H}(t-\tau)}d\tau, \tag{11}$$

which, upon substitution into the right-hand side of Eq. (9), yields

$$\frac{d\sigma(t)}{dt} = -i[\hat{H},\sigma(t)] - \lim_{N\to\infty}\frac{1}{N}\sum_{k=1}^{N}\int_0^t [\hat{W}(q_k(t)),e^{-i\hat{H}(t-\tau)} \times[\hat{W}(q_k(\tau)),\sigma(\tau)]e^{i\hat{H}(t-\tau)}]d\tau. \tag{12}$$

Then, assuming for the sake of simplicity bilinear QDS–bath coupling,

$$\hat{W}(q) = \hat{V}B(q), \tag{13}$$

we get

$$\frac{d\sigma(t)}{dt} = -i[\hat{H},\sigma(t)] - \int_0^t [\hat{V},e^{-i\hat{H}(t-\tau)} \times[\hat{V},\sigma(\tau)]e^{i\hat{H}(t-\tau)}]\mathcal{J}(t-\tau)d\tau, \tag{14}$$

where $\mathcal{J}(t-\tau)$ is determined via the MD recipe to calculate the classical correlation function,

$$\mathcal{J}(t-\tau) = \lim_{N\to\infty}\frac{1}{N}\sum_{k=1}^{N} B(q_k(t))B(q_k(\tau)). \tag{15}$$

Here the translational invariance of the correlation function is provided by the equilibrium state of the bath.

On the other hand, the formal solution of Eq. (4) is readily found using the two-dimensional probability density $\varphi(q,q';t)$ of the generalized set of coordinates q at time t given q' at time $t=0$, which satisfy

$$\left(\frac{\partial}{\partial t} - \mathcal{L}_q\right)\varphi(q,q';t) = 0\,, \quad \varphi(q,q';0) = \delta(q-q'). \tag{16}$$

Then the solution of Eq. (4) in the high temperature limit takes the form,

$$\eta(q,t) = -i\int_0^t\int \varphi(q,q';t-\tau)e^{-i\hat{H}(t-\tau)} \times[\hat{W}(q'),\sigma(\tau)]e^{i\hat{H}(t-\tau)}d\tau dq'. \tag{17}$$

Substituting Eq. (17) into the right-hand side of Eq. (3), and using bilinear QDS–bath coupling (13), we get Eq. (14) where the classical correlation function is defined as

$$\mathcal{J}(t-\tau) = \int\int B(q)\varphi(q,q';t-\tau)B(q')dqdq'. \tag{18}$$

Thus, Eqs. (3), (4) and (9), (10) differ only with respect to the recipe used to determine the classical correlation function.

The total number of MD trajectories needed to get accurate results depends on the specific system, but normally varies from several hundreds to thousands. The simultaneous solution of the large number of differential equations is very demanding with respect to the capacity of computer memory and inconvenient from a practical point of view. In addition, increasing the number of MD trajectories to improve the solution would require a complete recalculation of the time evolution.

In the classical nonequilibrium MD approach the solutions are found along single MD trajectories with subsequent averaging of the results. In other words, in NEMD averaging over an ensemble of MD trajectories is performed after propagation in time. However, the NQCA-MD approach, given by Eqs. (9) and (10), requires simultaneous solution along all MD trajectories involved in the calculation. Nevertheless, in practice, the number of simultaneously used MD trajectories can be reduced as follows. First, we introduce the solution of Eqs. (9) and (10) for a finite number (M) of MD trajectories. For simplicity we restrict ourselves again to the high temperature limit and transform the resulting equations into equivalent integrodifferential form. The result is almost identical to Eq. (12), but contains partially averaged (over given subset of MD trajectories) RDMs on both sides, i.e.,

$$\frac{d\sigma_M(t)}{dt} = -i[\hat{H},\sigma_M(t)] - \frac{1}{M}\sum_{k=1}^{M}\int_0^t [\hat{W}(q_k(t)),e^{-i\hat{H}(t-\tau)} \times[\hat{W}(q_k(\tau)),\sigma_M(\tau)]e^{i\hat{H}(t-\tau)}]d\tau. \tag{19}$$

One may add more trajectories to the average employing the formula,

$$\sigma_{M+L}(t) = \frac{M\sigma_M(t) + L\sigma_L(t)}{M+L}, \tag{20}$$

where the solutions are properly weighted. The average of Eq. (19) over all MD trajectories [by adding more partial averages using Eq. (20)] gives proper results only, if one can neglect the correlation between σ_M and the subset of MD trajectories in the integrand on the right-hand side of Eq. (19). Although it is clear, that increasing the number of MD trajectories in the partial average reduces undesirable correlations (making them negligibly small when $M\to\infty$), it is difficult to say *a priori* how many trajectories (say $N=10$, 50, or 100) will sufficiently reduce correlations between partially averaged RDMs and the subset of MD trajectories to treat the remaining correlations perturbatively (which are subsequently eliminated by adding more partial averages into the result). This number depends on the specific system investigated and can be estimated by comparing calculations with different numbers of MD trajectories going into partial averages.

It is known that quantum corrections[33,34] to the classical correlation functions may be very important, especially in the high frequency region. In principle, our NQCA-MD approach allows to incorporate this effect. In that case the true

MD trajectories should be replaced by the generic ones to reproduce the desired (corrected) correlation function by recipe (15), see Ref. 35 for details.

III. BREAKDOWN OF THE EXTERNAL FIELD APPROACH

A widely used approach to describe the dynamics of open quantum systems is based upon modeling the system–bath coupling in terms of a stochastically fluctuating external field that induces transitions within the QDS. However, as we show below, this method gives rise to relaxation processes that are fundamentally different from those obtained by invoking QDS–bath interactions explicitly on a molecular basis.

To demonstrate this qualitative difference, first we consider a simple two-level system, characterized by a QDS Hamiltonian $\hat{H}$ and an off-diagonal perturbation $\hat{V}$, in the presence of a phase relaxation process with a characteristic time τ_c due to interaction with the external subsystem,

$$\hat{H}=\frac{1}{2}\begin{pmatrix}-\omega_0 & 0\\ 0 & \omega_0\end{pmatrix}, \quad \hat{V}=\frac{1}{2}\begin{pmatrix}0 & V_0\\ V_0 & 0\end{pmatrix}. \tag{21}$$

The corresponding equations of motion for the elements of the density matrix are

$$\dot{n}(t)=iV_0(\sigma_{12}(t)-\sigma_{21}(t)), \tag{22}$$

$$\dot{\sigma}_{12}(t)=i\omega_0\sigma_{12}(t)+iV_0 n(t)/2-\sigma_{12}(t)/\tau_c, \tag{23}$$

$$\dot{\sigma}_{21}(t)=-i\omega_0\sigma_{21}(t)-iV_0 n(t)/2-\sigma_{21}(t)/\tau_c, \tag{24}$$

where

$$n(t)=\sigma_{11}(t)-\sigma_{22}(t) \tag{25}$$

is the population difference. It is readily seen from Eqs. (22) to (24) that transitions between the states of the system are caused by the corresponding off-diagonal elements which coherently couple the two states. Indeed, when $\sigma_{12}(t)-\sigma_{21}(t)=0$, the time derivative of the population difference is zero. Similarly, increasing the relaxation rate of the off-diagonal elements decreases rate of transitions and vice versa.

The situation looks different in a phenomenological rate description, which results in a closed set of equations for energy levels populations. Although the off-diagonal elements of the density matrix do not appear in this approach, it is implicitly assumed that they are negligibly small. To illustrate this we write the solution of Eq. (23) as

$$\sigma_{12}(t)=\frac{iV_0}{2}\int_0^t e^{(i\omega_0-1/\tau_c)\tau}n(t-\tau)d\tau, \tag{26}$$

which, upon substitution into Eq. (22), yields a closed non-Markovian equation for the population difference [$\sigma_{21}(t)$ is given by complex conjugate of Eq. (26)],

$$\dot{n}(t)=-V_0^2\int_0^t e^{-\tau/\tau_c}\cos(\omega_0\tau)n(t-\tau)d\tau. \tag{27}$$

A rate description is only valid in the Markovian limit, which is attained if one assumes small changes of $n(t-\tau)$ at $\tau \sim \tau_c$ and $t \gg \tau_c$. In that case one may replace $n(t-\tau)$ by $n(t)$ in Eq. (27), and replace the upper limit of integral by infinity to get

$$\dot{n}(t)=-Kn(t), \quad K=\frac{V_0^2\tau_c}{1+\omega_0^2\tau_c 2}, \quad K\tau_c \ll 1, \tag{28}$$

where the last condition is introduced for self-consistency to ensure a small change of the population difference on the time scale of τ_c. Thus, a rate description does not imply the absence of corresponding off-diagonal density matrix elements, they are inavoidably created during transitions between energy levels.

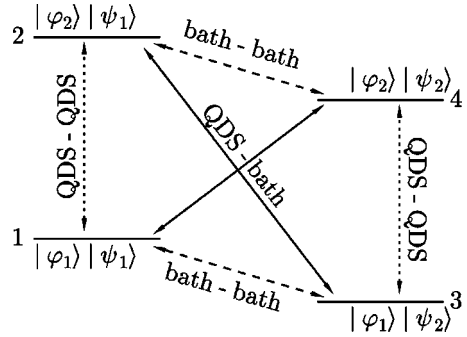

FIG. 1. Energy levels of a four-level system in the basis of direct product states of QDS ($|\varphi_{1,2}\rangle$) and bath states ($|\psi_{1,2}\rangle$). Dotted arrows show transitions between states of the QDS, dashed arrows, between bath states, while solid arrows show cross transitions between QDS and bath states.

We now turn to a four-level system as shown in Fig. 1, where both QDS and bath have only 2 levels. As a basis we use the direct product of states of the QDS ($|\varphi_{1,2}\rangle$) and of the bath ($|\psi_{1,2}\rangle$) and indicate different types of transitions. Dotted arrows show transitions inside the QDS (the state of the bath is not changed), dashed ones show transitions inside the bath (no changes in QDS state), while solid arrows indicate transitions at the expense of QDS–bath interactions (when both the states of the QDS and the bath are changed). It is the latter process that is responsible for the relaxation of energy levels in the quantum-classical approximation developed here.

As we demonstrated above, the corresponding off-diagonal elements are always created during transitions, and are shown below in the total density matrix ϱ using the same line types as in Fig. 1,

$$\varrho=\begin{pmatrix}\varrho_{11} & \varrho_{12} & \varrho_{13} & \boxed{\varrho_{13}}\\ \varrho_{21} & \varrho_{22} & \boxed{\varrho_{23}} & \varrho_{24}\\ \varrho_{31} & \boxed{\varrho_{32}} & \varrho_{33} & \varrho_{34}\\ \boxed{\varrho_{41}} & \varrho_{42} & \varrho_{43} & \varrho_{44}\end{pmatrix}. \tag{29}$$

On the other hand, the corresponding reduced density matrix of the QDS, obtained by taking partial trace over bath states is of the form,

$$\sigma=\begin{pmatrix}\varrho_{11}+\varrho_{33} & \varrho_{12}+\varrho_{34}\\ \varrho_{21}+\varrho_{43} & \varrho_{22}+\varrho_{44}\end{pmatrix}. \tag{30}$$

This means, that off-diagonal elements involving transitions due to QDS–bath and bath–bath interactions do not appear in the reduced density matrix of the QDS.

Our quantum-classical approximation is in agreement with these results. Indeed, the QDS–bath interaction Hamiltonian $\hat{W}(q)$ creates off-diagonal elements in the auxiliary matrix η, but not in the QDS density matrix σ, see Eqs. (3), (4) or Eqs. (9), (10). There is no coherently driven bath induced transition between QDS states. The situation is qualitatively different if QDS–bath interactions are modeled by a time-dependent QDS Hamiltonian in the framework of a Liouville or Schrödinger equation. In that case the transitions are induced directly by the fluctuating field between the states of the QDS, and, therefore, off-diagonal elements (coherence) between the states of the QDS appear, which is unphysical for the relaxation process under consideration.

The external field approach can, however, provide a correct description of the populations dynamics due to QDS–bath interactions in cases where off-diagonal elements in the reduced density matrix are initially small and not efficiently created during relaxation. If this is not the case (initial coherent state and/or non-Markovian relaxation, for instance) the external field approach fails to describe relaxation kinetics properly. For example, an initially coherent state of the QDS, in reality, does not directly affect the rate of cross transitions between QDS and bath, but strongly accelerates them within the external field approach.

IV. MOLECULAR DYNAMICS SIMULATIONS

We now consider the VER of a breathing sphere in a Lennard-Jones (LJ) fluid, i.e., our model involves a single vibrating solute particle which interacts with the solvent particles through a spherically symmetric pair potential $\phi_u(r,q)$, where x is vibrational coordinate, while r is the solute–solvent distance.[32,36] (Some notations used in this section interfere with those used in the formulation of NQCA. However, the use of σ to denote particle diameter has a long tradition in the field of MD simulations of LJ fluids.)

The solvent molecules interact via the familiar LJ potential,

$$\phi_v(r_{ij})=4\varepsilon_v\left[\left(\frac{\sigma_v}{r_{ij}}\right)^{12}-\left(\frac{\sigma_v}{r_{ij}}\right)^{6}\right], \tag{31}$$

where ε_v is the well depth, σ_v is the effective diameter of the solvent particle, while r_{ij} is the distance between solvent molecules. In turn, the solute–solvent interaction is defined as

$$\phi_u(x,r_{1j})=4\varepsilon\left[\left(\frac{\sigma}{r_{1j}-x/2}\right)^{12}-\left(\frac{\sigma}{r_{1j}-x/2}\right)^{6}\right], \tag{32}$$

where $\varepsilon=\sqrt{\varepsilon_v\varepsilon_u}$, $\sigma=(\sigma_v+\sigma_u)/2$, and ε_u and σ_u are solute–solute well depth and diameter, respectively.

The amplitude of the breathing sphere oscillations is assumed to be small compared with its equilibrium radius R_0, which allows to approximate describe the breathing sphere motion using a harmonic potential. Finally, the total Hamiltonian of the N particle system is

$$H=\frac{1}{2}\mu\dot{x}^2+\frac{1}{2}\mu\omega_0^2x^2+\frac{1}{2}m_u\dot{r}_1^2+\frac{1}{2}m_v\sum_{j=2}^{N}\dot{r}_j^2 +\sum_{j=2}^{N}\phi_u(r_{1j},x)+\sum_{i=2}^{N-1}\sum_{j=i+1}^{N}\phi_v(r_{1j}). \tag{33}$$

Here the first line represents the Hamiltonian for the vibrational coordinate of the breathing sphere, where μ and ω_0 are the reduced mass and the angular frequency, correspondingly. The second line contains the total kinetic energy of solute and solvent particles, with masses of m_u (solute) and m_v. The solute–solvent interactions are collected in the last line of Eq. (33).

Coupling between the solute vibrational mode and the external degrees of freedom is provided by the force,

$$F_x(q)=\sum_{j=2}^{N}f(r_{1j},x), \tag{34}$$

where q denotes the generalized set of coordinates of bath particles, and

$$f(r_{1j},x)=-\frac{\partial\phi_u(r_{1j},x)}{\partial x} =-\frac{12\varepsilon}{r_{1j}-x/2}\left[2\left(\frac{\sigma}{r_{1j}-x/2}\right)^{12}-\left(\frac{\sigma}{r_{1j}-x/2}\right)^{6}\right]. \tag{35}$$

The MD calculations were carried out using 500 particles (including one representing the breathing sphere) at constant volume and energy in a cubic simulation box with periodic boundary conditions. Potentials were truncated at half the box length and replaced by ''shifted-force-potentials'' [37,38] of the form,

$$V^{\mathrm{SF}}(r)=\left[V(r)-V(R_c)-\left.\frac{dV(r)}{dr}\right|_{r=R_c}(r-R_c)\right]\theta(R_c-r), \tag{36}$$

to keep forces continuous at the cutoff distance R_c.

The parameters chosen are chosen to mimick the vibrational relaxation of iodine in argon at liquidlike density and room temperature. The LJ-parameters of argon are $\varepsilon_v/k=119.9$ K and $\sigma_v=0.3405$ nm, the argon mass $m_v=39.95$ g/mol. For the solute we take $\varepsilon/k=187.5$ K, $\sigma_u=0.3617$ nm, $m_u=253.8$ g/mol, and $\mu=m_u/4$. The vibrational frequency of the solute molecule $\omega_0/(2\pi c)=220\ \mathrm{cm}^{-1}$ corresponds to the gas phase vibrational frequency of iodine. Temperature and density were adjusted to $T=300$ K and $\rho=19.0\ \mathrm{nm}^{-3}$, which correspond to $T^*=kT/\varepsilon_v=2.5$ and $\rho^*=\rho\sigma_v^3=0.75$ in reduced LJ units.

Classical simulations of the VER of the breathing sphere were performed on the basis of the nonequilibrium molecular dynamics approach. For integration the leapfrog Verlet algorithm with a time step of $\Delta t=2$ fs was used. Initially, the system was equilibrated as follows. Starting from a face centered cubic structure with initial velocities corresponding to 400 K, we rescaled the velocities after 10^4 time steps to reach the desired temperature of 300 K. Subsequently, the system was further equilibrated for 100 ps. Then, from the

running equilibrium simulation a pool of 300 starting configurations was generated by repeatedly storing configurations every 10 ps. For each starting configuration excitation of the breathing sphere was achieved by increasing its kinetic vibrational energy by 1100 cm^{-1} (corresponding to 5 vibrational quanta). The subsequent relaxation of the vibrational energy was monitored for ~ 70 ps and averaged.

V. QUANTUM-CLASSICAL SIMULATIONS

The Hamiltonian of the QDS is given by ($\hbar=1$)

$$\hat{H}=-\frac{1}{2\mu}\frac{d^2}{dx^2}+\frac{\mu\omega_0 x^2}{2}, \tag{37}$$

where ω_0 and μ are oscillator frequency and mass, respectively. It is a quantum mechanical analog of the first line of Eq. (33). The energy levels E_n (eigenvalues) and the corresponding eigenfunctions $|\psi\rangle_n$ are readily determined by solving the stationary Schrödinger equation,

$$\hat{H}|\psi\rangle_n=E_n|\psi\rangle_n. \tag{38}$$

By introducing creation ($\hat{a}_+$) and annihilation ($\hat{a}_-$) operators, defined by the standard relations,

$$\hat{a}_\pm=\sqrt{\frac{\mu\omega_0}{2}}\left(x\mp\frac{i\hat{p}}{\mu\omega_0}\right), \tag{39}$$

the QDS Hamiltonian (37) is rewritten as

$$\hat{H}=\omega_0(\hat{a}_+\hat{a}_-+\tfrac{1}{2}). \tag{40}$$

The coupling between QDS and bath is effected by the interaction potential,

$$\Phi(x)=\sum_{j=2}^{N}\phi_u(r_{1j},x), \tag{41}$$

which can be expanded in the vicinity of $x=0$ to give

$$\begin{aligned}\Phi(x,q)&\simeq\Phi(0,q)+\left.\frac{\partial\Phi(x,q)}{\partial x}\right|_{x=0}x+\cdots\\&=\Phi(q)+F_0(q)x+\cdots.\end{aligned} \tag{42}$$

Thus, the QDS–bath coupling Hamiltonian takes the form,

$$\begin{aligned}&\hat{W}(q(t))=(\hat{a}_++\hat{a}_-)B(q(t)),\\&B(q(t))=\sqrt{\frac{1}{2\mu\omega_0}}F_0(q(t)),\end{aligned} \tag{43}$$

where the internal vibrational coordinate is treated quantum-mechanically, and expressed via creation/annihilation operators (40). Finally, the matrix elements of the QDS Hamiltonian and of the QDS–bath coupling in the basis of eigenstates of $\hat{H}$ are ($k,n=0,1,2,\ldots$),

$$\begin{aligned}&\hat{H}_{kn}=\omega_0(n+\tfrac{1}{2})\delta_{kn},\\&\hat{W}_{kn}(q(t))=(\sqrt{n+1}\,\delta_{k,n+1}+\sqrt{k+1}\,\delta_{k+1,n})B(q(t)).\end{aligned} \tag{44}$$

Thus, for quantum-classical simulations (NQCA-MD) of the VER one needs the perturbing force $F_0(q(t))$, see Eqs. (34), (35), and (43), as a function of time. Since feedback between the QDS and the bath is neglected, the time series of the force was generated by equilibrium MD simulations with the oscillator coordinate held fixed at its equilibrium radius, i.e., with $x=0$ in Eq. (35). Note, however, that both NQCA-MD and NEMD are non-Markovian approaches and hence not equivalent to a rate description where relaxation rates are determined by the Fourier transforms of the equilibrium correlation function at the transition frequencies. All other simulation parameters were the same as for NEMD simulations, see Sec. IV.

VI. RESULTS AND DISCUSSION

In this section we compare the results of NQCA-MD simulations of the VER kinetics of a breathing sphere with those from the purely classical NEMD simulation. The energy of the solute within quantum-classical treatments is not well defined, as an arbitrary constant multiplied by the unit operator may be added to the quantum Hamiltonian. It is convenient to define the energy in such a way as to have the equilibrium (relaxed) energy of the QDS equal to T (we continue with $\hbar=k_B=1$),

$$\begin{aligned}&E(t)=E^{\mathrm{QDS}}(t)-E^{\mathrm{QDS}}_{\mathrm{eq}}+T,\\&E^{\mathrm{QDS}}_{\mathrm{eq}}=\sum_{j=1}^{N_q}E_j e^{-E_j/T}\Big/\sum_{j=1}^{N_q}e^{-E_j/T}.\end{aligned} \tag{45}$$

This definition is independent of a common shift of energy levels. Here N_q is the number of quantum states included.

Two types of initial conditions will be used for the quantum-dynamical subsystem: (i) an eigenstate (delocalized state) and (ii) a coherent state (minimum uncertainty state) of the harmonic oscillator,

$$|\varphi\rangle=e^{-|\alpha|^2/2}\sum_{n=0}^{\infty}\frac{\alpha^n}{\sqrt{n!}}|n\rangle. \tag{46}$$

Here α is some complex parameter determining energy and other characteristics (average position and momentum) of the coherent state, while $|n\rangle$ is the corresponding normalized eigenstate of Hamiltonian (40). The RDM of the coherent state is of the form,

$$\sigma_{nm}=e^{-|\alpha|^2}\frac{\alpha^n(\alpha^*)^m}{\sqrt{n!m!}}. \tag{47}$$

We used, however, a slightly renormalized definition yielding unit trace of the density matrix for the finite number of basis functions considered here, i.e., in our case we take

$$\sigma_{nm}=\frac{\alpha^n(\alpha^*)^m}{\sqrt{n!m!}}\Big/\sum_{l=0}^{N_q}\frac{|\alpha|^{2l}}{l!}. \tag{48}$$

A preliminary analysis of the bath dynamics shows, that a LJ fluid has both high and slow frequency modes. The former are readily demonstrated by calculating the force correlation function at short times, shown in Fig. 2 [via MD recipe (15), see also Eq. (43)]. The existence of low-frequency modes is more easily shown by plotting the value

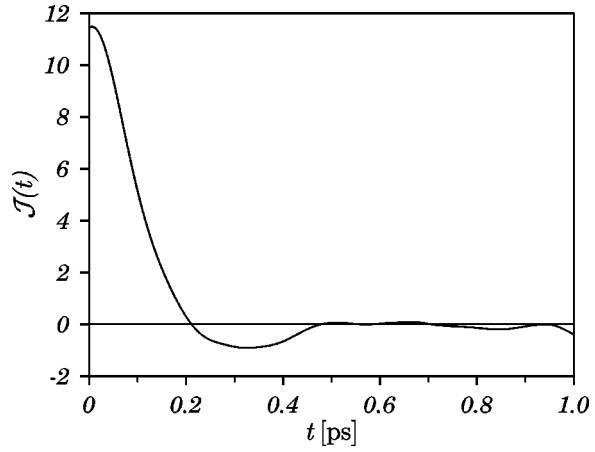

FIG. 2. Force correlation function $\mathcal{J}(t)$ as the function of time, see Eq. (15), obtained after averaging over 1600 MD trajectories.

$$\mu(t)=\int_0^t (B(q(\tau))-\overline{B})d\tau, \quad \overline{B}=\lim_{T\to\infty}\frac{1}{T}\int_0^T B(q(\tau))d\tau \tag{49}$$

along several MD trajectories. Here $\overline{B}$ is an average force acting on the breathing sphere, which in the limit of large times does not depend on MD trajectory. If low-frequency modes are absent, the parameter $\mu(t)$ should fluctuate around zero with an average period of about 1 ps. This is obviously not the case, see Fig. 3.

The high frequency modes of LJ solvent for the given parameter values have rather short correlation time of about 0.2 ps. Also the transition frequencies are equal to each other (equidistant energy spectrum of harmonic oscillator, while the transitions are induced only between neighboring levels) and have relatively high values: $(220\ \mathrm{cm}^{-1}=4.136\times10^{13}$ rad/s). This means that only the short-time dynamics of the LJ fluid contributes to the relaxation process. However, for quantum subsystems involving small energy splittings, low-frequency solvent modes may play a decisive role and even lead to non-Markovian relaxation, as the correlation times for low-frequency modes usually are longer.

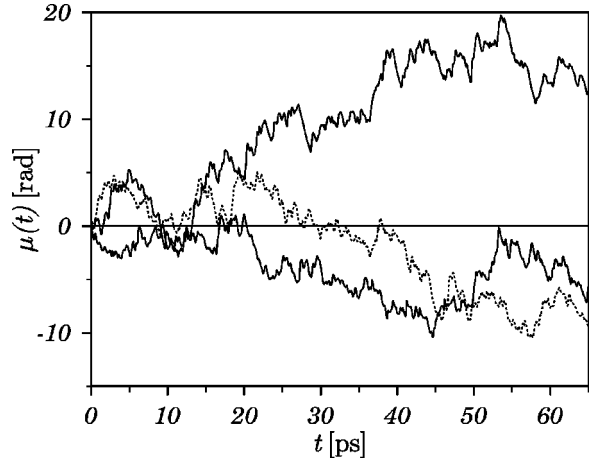

FIG. 3. Demonstration of low-frequency modes in the dynamics of LJ fluid. The parameter $\mu(t)$, see Eq. (49), is plotted along several MD trajectories.

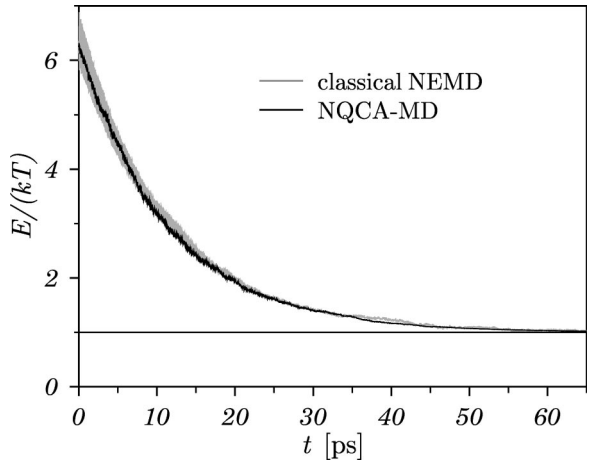

FIG. 4. Comparison between pure classical NEMD simulations of vibrational energy relaxation of breathing sphere in LJ fluid with the NQCA-MD (500 trajectories) results.

We now compare results of purely classical NEMD simulations of vibrational energy relaxation with corresponding results from the NQCA-MD approach. We start from a coherent state with $\alpha=5.5$ to adjust the initial energy of the QDS ($\omega_0(1/2+\alpha)$) to the initial energy used in the NEMD simulations. We used sets of 50 trajectories in NQCA-MD for partial averages. Figure 4 illustrates the good agreement between the purely classical NEMD and the NQCA-MD treatments of the VER.

For the breathing sphere in a LJ fluid there exists a nonzero time averaged force. Usually it is eliminated by the corresponding renormalization of the QDS Hamiltonian and the QDS–bath interaction in such a way that the latter has zero time averaged value and is called "fluctuating force." Although the above procedure looks reasonable, it cannot be justified within the frameworks of quantum-classical treatment. Indeed, our approach requires a potential renormalization of the form,

$$\hat{H}\to\hat{H}+\mathrm{Tr}_b(\hat{W}\rho_b), \quad \hat{W}\to\hat{W}-\mathrm{Tr}_b(\hat{W}\rho_b), \tag{50}$$

where ρ_b is the density matrix of the canonical bath and the trace is taken only over bath variables, see Ref. 27 for more details. Otherwise the generalized non-Markovian master equation would contain a long lasting source term due to the initial correlations, which compensates the improper choice of the memory kernel and causes subsequent approximations to be hardly possible.

However, the renormalization (50) was introduced using a quantum-mechanical description of the bath degrees of freedom. In that case one has (in the basis diagonalizing the bath Hamiltonian, $\mathcal{E}_\alpha$ its eigenvalues),

$$\mathrm{Tr}_b(\hat{W}\rho_b)=\frac{1}{Z_b}\sum_\alpha \hat{W}^{\alpha\alpha}e^{-\mathcal{E}_\alpha/T}, \quad Z_b=\sum_\alpha e^{-\mathcal{E}_\alpha/T}, \tag{51}$$

where Greek letters designate matrix elements between bath states. Within the quantum-classical treatments one deals with some Hamiltonian $\hat{W}(q)$ with matrix elements in the QDS subspace depending parametrically on the generalized set of phase space coordinates q. It is frequently assumed,

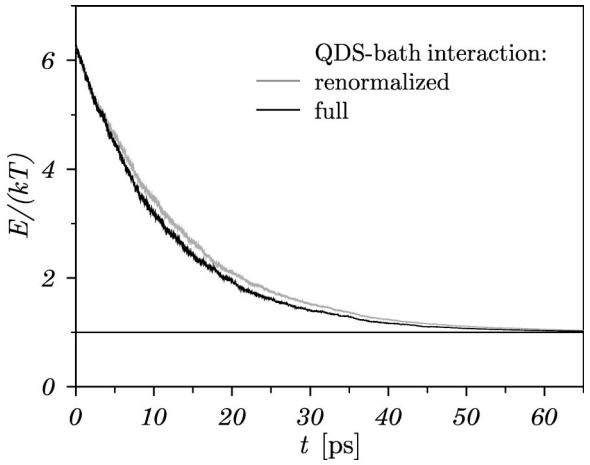

FIG. 5. Influence of the renormalization of the QDS–bath interaction on the relaxation kinetics produced by NQCA-MD. Gray line corresponds to the case when time average force is included into the QDS Hamiltonian (the QDS–bath interaction contains only the fluctuating part, with zero time average). Black line shows the kinetics calculated with full QDS–bath interaction.

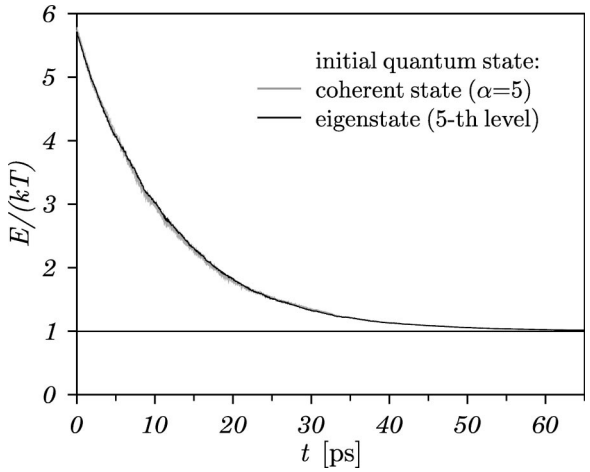

FIG. 6. VER kinetics for the coherent initial state ($\alpha=5$, gray line) vs initial eigenstate (fifth eigenstate, black line). NQCA-MD for both calculations utilized the same set of 500 MD trajectories.

that in this case the integration of $\hat{W}(q)$ over phase space coordinates is the direct analog of taking the trace over bath variables, i.e., that

$$\mathrm{Tr}_b(\hat{W})=\int \hat{W}(q)dq=\lim_{t\to\infty}\frac{1}{t}\int_0^t \hat{W}(q(\tau))d\tau, \tag{52}$$

where the last definition corresponds to the MD recipe, where integration over phase space can be replaced by averaging over a sufficiently long time to entirely explore the phase space.

Although Eq. (52) looks reasonable, it is not equivalent to the original definition of the trace, given by Eq. (51). Indeed, from Eq. (51) it follows, that the renormalization concerns only the diagonal of the bath variables part of the QDS–bath Hamiltonian. In other words, only that part of the QDS–bath Hamiltonian, which *does not induce* transitions between bath states is included into the renormalization. The ''classical'' definitions (52), however, do not account for this fact. In our case the QDS–bath interaction Hamiltonian is given by Eq. (43) and has no diagonal part. But the transitions induced by such a Hamiltonian are necessarily accompanied by transitions between bath states (the QDS either receives energy from or gives it to the bath). Thus, as follows from the quantum-mechanical definition (51), the Hamiltonian (43) does not lead to renormalization. The ''classical'' analog of the partial trace (52), however, leads to the opposite conclusion. Besides, Eq. (52) treats time averaged QDS–bath interaction as an external field, which introduces improper coherencies into the QDS, see Sec. III. Thus, based on the above analysis, we conclude, that for the QDS–bath Hamiltonian in use, see Eq. (43), the renormalization should not be done.

The contribution of the time averaged force into relaxation kinetics for the system under consideration is shown in Fig. 5. In the first case (gray line) the average force is included into the QDS Hamiltonian, and the QDS–bath interaction contains only its fluctuating part, see Eqs. (50) and (52). In the second case (black line) the renormalization was not used. The parameter α, defining the energy of the initial coherent state was 5.5 in the latter case, but was reduced to 5.2 in the former case to provide the same initial energy for the QDSs (the renormalization of the QDS Hamiltonian slightly changes the initial energy). There exists a pronounced difference between the results. In particular, fitting of the kinetics by a single exponential decay of the form,

$$E(t)/T=1.0+Ae^{-t/\tau} \tag{53}$$

yields $A=5.3$ in both cases, $\tau=11.5$ ps without renormalization and $\tau=13$ ps otherwise, i.e., the renormalization for the considered model leads to the 12% longer relaxation time. The same procedure, applied to the NEMD kinetics after smoothing the curve, gives $\tau=11.7$ ps.

The above analysis fundamentally questions the accuracy of the Markovian approximation, as it appears not to be well defined if the force correlation function does not decay to zero. In contrast, in view of their non-Markovian nature, neither our NQCA-MD nor NEMD approaches suffer from this problem.

It has been shown,[39] that the applicability of different approaches used to theoretically describe VER dynamics may depend on the initial conditions. Although the final (relaxed) state must be independent of the initial state of the system, the influence of the initial coherence on VER kinetics of a harmonic oscillator has to be analyzed. Figure 6 shows the comparison between VER kinetics for a coherent state (47) with $|\alpha|^2=5$, and the fifth eigenstate of the harmonic oscillator as initial state. The difference between the two relaxation curves is hardly visible in Fig. 6. Thus the initial coherence has no noticeable effect on the energy relaxation of the harmonic oscillator. (In both calculations we utilized the same set of 500 MD trajectories.)

A NQCA-MD simulation of VER gives more detailed information about the state of the QDS than purely classical NEMD. Figures 7(a) and 7(b) show the dynamics of individual vibrational level populations for the two types of the initial conditions considered above. Starting from the fifth

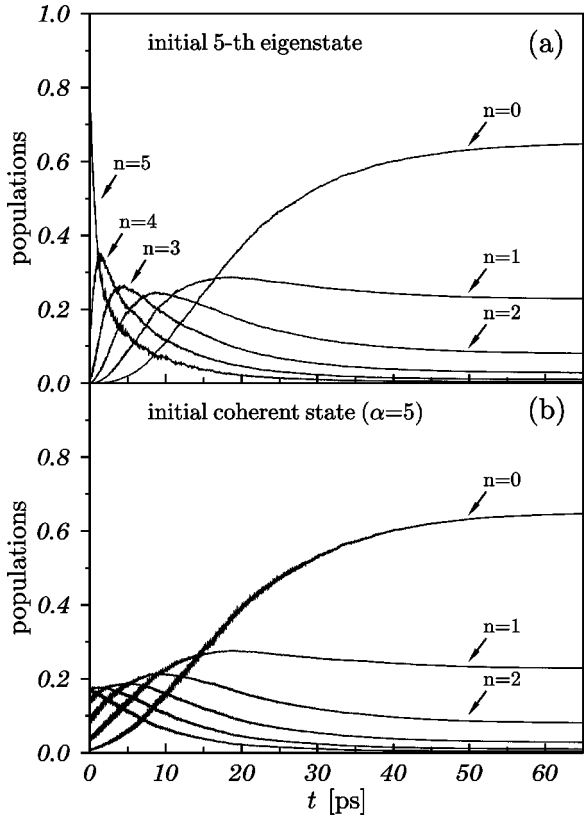

FIG. 7. Evolution of the populations of energy levels. Two types of initial conditions with the same initial energy are used, in case (a) the eigenstate number 5 was originally populated, while case (b) corresponds to the initial coherent state with $\alpha=5$.

eigenstate [see Fig. 7(a)], its population relaxes monotonously, while that of the fourth level first increases, and then decays to its equilibrium value. Similar behavior is observed for the lower levels, only their increase appears at later times. This happens because the QDS–bath coupling, see Eq. (44), has nonzero matrix elements only between neighboring states. In this way, the ground state has the longest incubation time, after which its population increases nearly monotonously to its equilibrium value. Starting from a coherent state, [Fig. 7(b)], the differences between the time evolution of individual level population become less pronounced, as all of them already contribute more or less to the initial state. For example, the incubation time of the ground state becomes shorter since neighboring levels are slightly populated already initially.

Finally, we analyze the time dependent loss of coherence of the initial coherent state. For this purpose we plot the uncertainty product of the state, defined as

$$\Delta x \Delta p = \sqrt{\overline{x^2}-\overline{x}^2}\sqrt{\overline{p^2}-\overline{p}^2}. \tag{54}$$

It is well known, that the coherent state is a minimum uncertainty state, i.e., that it obeys $\Delta x \Delta p = \hbar/2$. In contrast, if only some diagonal element n of the RDM is nonzero, one has $\Delta x \Delta p = \hbar(n+1/2)$. Thus, the uncertainty is a convenient measure of the extent of coherence in a given state. Figure 8 shows its time evolution starting from an initially coherent state with $\alpha=5$. Initially, the uncertainty is $\hbar/2$.

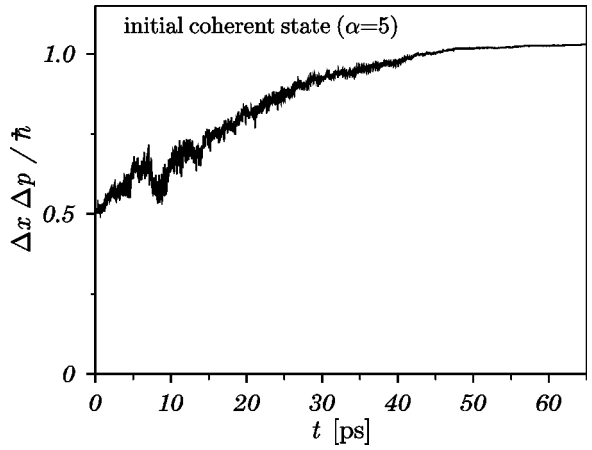

FIG. 8. Evolution of the uncertainty for the initial coherent state with $\alpha=5$.

Within the first ~ 15 ps the evolution of the uncertainty is nonmonotonous, after that it increases rather smoothly to its equilibrium value equal to 1.036 $\hbar$.

VII. CONCLUSION

In the present article we developed an efficient method to solve equations of our novel non-Markovian quantum-classical approximation[27] directly in the time domain by using the molecular dynamics method for *ab initio* simulation of the dynamics of the classical bath. This NQCA-MD approach gives an accurate and physically sound description of various characteristics of an open quantum model system coupled to a dissipative environment. The close agreement between the VER kinetics obtained from nonequilibrium classical MD simulations and from our NQCA-MD approach provides evidence for the accuracy of the new method. On the other hand, the close agreement between classical and quantum-classical descriptions of VER could be the result of peculiar features of the one-dimensional harmonic oscillator employed as a model. One might expect, therefore, that for more realistic and complex open quantum systems there will be significant deviations between results from purely classical and quantum-classical modeling of the VER.

Several aspects of quantum-classical treatments were discussed throughout the article. In particular, the widely used approach to model the system–bath interaction as a fluctuating external force field and within the framework of Schrödinger or Liouville equations does not correctly treat the system–bath correlations and introduces improper coherence between the states of the quantum subsystem. As a result, the external field approach fails to describe non-Markovian relaxation and/or the case of large initial coherence in the quantum subsystem, see also Sec. III. Another aspect is the absence of the well-defined Markovian limit in the presence of a nonzero time averaged force, which appears to be properly handled only within non-Markovian approaches.

ACKNOWLEDGMENT

One of the authors (A.A.N.) is grateful to the Alexander von Humboldt Foundation for a postdoctorate fellowship.

APPENDIX: NUMERICAL IMPLEMENTATION

Our numerical approach employes the standard leapfrog algorithm. The time dependence of the QDS–bath coupling $\hat{W}(q(t))$ is represented as a series of switching Hamiltonians, where the time between switches is equal to the time step Δt. The numerical integration of Eqs. (9) and (10) presents certain difficulties caused by fast oscillation of the off-diagonal elements of the density and auxiliary matrices. To overcome the problem, we introduce ''slow'' matrices by switching to the interaction representation,

$$\xi(t)=e^{i\hat{H}t}\sigma(t)e^{-i\hat{H}t}, \quad \phi_k(t)=e^{i\hat{H}t}\eta_k(t)e^{-i\hat{H}t}. \tag{A1}$$

They satisfy the following set of equations which are readily obtained from Eqs. (9), (10), and (A1),

$$\frac{d\xi(t)}{dt}=-\frac{1}{M}\sum_{k=1}^{M} i[\hat{W}^k(t),\phi_k(t)], \tag{A2}$$

$$\frac{d\phi_k(t)}{dt}=-i[\hat{W}^k(t),\xi(t)]+[\hat{U}^k(t),\xi(t)]_+ +\left[\hat{Y}^k(t),\frac{d\xi(t)}{dt}\right]_+, \tag{A3}$$

and with the same initial conditions, as in Eqs. (9) and (10). Here M is the number of MD trajectories used for partial average, and

$$\begin{aligned}\hat{W}^k(t)&=e^{i\hat{H}t}\hat{W}(q_k(t))e^{-i\hat{H}t},\\ \hat{U}^k(t)&=e^{i\hat{H}t}\hat{U}(q_k(t))e^{-i\hat{H}t},\\ \hat{Y}^k(t)&=e^{i\hat{H}t}\hat{Y}(q_k(t))e^{-i\hat{H}t}\end{aligned} \tag{A4}$$

are operators in the interaction representation.

Since Eqs. (9) and (10) are local-time differential equations, we only need to construct a numerical method to propagate the solution on the length of a single time step (from 0 to Δt) and with a fixed set (corresponding to the given time step) of the QDS–bath couplings. The initial conditions for each time step are obtained from the preceding one [for the first time step they are given by Eq. (8)].

The evaluation of the right-hand sides of Eqs. (A2) and (A3) can be done using the results from the preceding time steps or using those from the current time step as well. The former schemes are called ''explicit'' and usually have poor stability and accuracy. The latter schemes are called ''implicit,'' they are more stable and accurate, but require the inversion of the Liouville space operator, which leads to unfavorable scaling. We propose a simple approach, intermediate between explicit and implicit integration schemes. It combines the stability of implicit scheme and easy evaluation of the right-hand sides provided by an explicit scheme. First, we integrate Eqs. (A2) and (A3) over the time step Δt and use the following approximations for the integrals ($\gamma=\xi,\phi$):

$$\begin{aligned}\int_0^{\Delta t}[\hat{W}^k(\tau),\gamma(\tau)]&\simeq[\hat{\tilde{W}}^k,\gamma(\Delta t)],\\ \int_0^{\Delta t}[\hat{U}^k(\tau),\xi(\tau)]_+&\simeq[\hat{\tilde{U}}^k,\xi(\Delta t)]_+,\end{aligned} \tag{A5}$$

and

$$\int_0^{\Delta t}\left[\hat{Y}^k(\tau),\frac{d\xi(\tau)}{d\tau}\right]_+\simeq\frac{1}{\Delta t}[\hat{\tilde{Y}}^k,\xi(\Delta t)-\sigma_0]_+, \tag{A6}$$

where the tilde denotes integrated over Δt operators, defined as

$$\begin{aligned}\hat{\tilde{W}}^k&=\int_0^{\Delta t}\hat{W}^k(\tau)d\tau, \quad \hat{\tilde{U}}^k=\int_0^{\Delta t}\hat{U}^k(\tau)d\tau,\\ \hat{\tilde{Y}}^k&=\int_0^{\Delta t}\hat{Y}^k(\tau)d\tau.\end{aligned} \tag{A7}$$

Then we get the following set of algebraic equations:

$$\xi=-\frac{1}{N}\sum_{k=1}^{N} i[\hat{\tilde{W}}^k,\phi_k]+\sigma_0, \tag{A8}$$

$$\phi_k=-i[\hat{\tilde{W}}^k,\xi]+[\hat{\tilde{U}}^k,\xi]_+ +\frac{1}{\Delta t}[\hat{\tilde{Y}}^k,\xi-\sigma_0]_+ +\eta_{0k}. \tag{A9}$$

Substituting Eq. (A9) in the right-hand side of Eq. (A8) we get a closed equation for determining ξ;

$$\xi=\hat{\Theta}(\xi)+\sigma_0, \quad \hat{\Theta}(\xi)=\frac{1}{M}\sum_{k=1}^{M}\hat{\Theta}^k(\xi), \tag{A10}$$

where

$$\hat{\Theta}^k(\xi)=-[\hat{\tilde{W}}^k,[\hat{\tilde{W}}^k,\xi]]-i[\hat{\tilde{W}}^k,[\hat{\tilde{U}}^k,\xi]_+] -\frac{i}{\Delta t}[\hat{\tilde{W}}^k,[\hat{\tilde{Y}}^k,\xi-\sigma_0]_+]-i[\hat{\tilde{W}}^k,\eta_{0k}]. \tag{A11}$$

Then, Eqs. (A10) and (A11) are solved in the *eigenbasis* of $\hat{H}$ as

$$\xi_{lm}^{(0)}=\frac{\hat{\Theta}_{lm}(\sigma_0)}{1+\hat{D}_{lm}}+\sigma_{0lm}, \quad \hat{D}=\frac{1}{M}\sum_{k=1}^{M}\hat{D}^k, \tag{A12}$$

where there is no summation over indices l and m, and matrices $\hat{D}^k$ has the following matrix elements:

$$\hat{D}_{lm}^k=(\hat{\tilde{W}}^k\hat{\tilde{W}}^k)_{ll}+(\hat{\tilde{W}}^k\hat{\tilde{W}}^k)_{mm}-2\hat{\tilde{W}}_{ll}^k\hat{\tilde{W}}_{mm}^k+i((\hat{\tilde{W}}^k\hat{\tilde{U}}^k)_{ll} -(\hat{\tilde{U}}^k\hat{\tilde{W}}^k)_{mm}+\hat{\tilde{W}}_{ll}^k\hat{\tilde{U}}_{mm}^k-\hat{\tilde{W}}_{mm}^k\hat{\tilde{U}}_{ll}^k). \tag{A13}$$

In other words, in the equation for ξ_{lm} we take from the right-hand side of Eq. (A11) the term containing ξ_{lm} as well, and treat it implicitly. It is readily seen, however, that the contribution from the third term in the right-hand side of Eq. (A11) is absent in $\hat{\Theta}^k(\sigma_0)$. To take it into account we substitute the obtained solution for $\xi^{(0)}$ into the above-mentioned term to get the corresponding correction to the solution, i.e.,

$$\xi=\xi^{(0)}-\frac{1}{\Delta t}\frac{1}{M}\sum_{k=1}^{M} i[\hat{\tilde{W}}^k,[\hat{\tilde{Y}}^k,\xi^{(0)}-\sigma_0]_+]. \tag{A14}$$

The solution obtained for ξ is then substituted into the right-hand side of Eq. (A9) to determine elements of ϕ_k. The resulting scheme is quite stable and computationally inexpensive as well. The accuracy and stability of the algorithm may be increased, but that would also increase computational cost.

The algorithm works as follows. At first, we use some appropriate basis and specify the matrix elements of the QDS Hamiltonian $\hat{H}$, and the initial conditions for the density matrix σ_0. After this, we diagonalize $\hat{H}$ and transform the initial conditions into the new basis. The transformation matrices and the eigenvalues of $\hat{H}$ are stored for subsequent use. We also calculate and store matrices a_{lm} and b_{lm}, defined by Eq. (6), vector $\mathbf{Z}$ with elements,

$$\mathbf{Z}=(e^{iE_1\Delta t},e^{iE_2\Delta t},\ldots), \tag{A15}$$

where E_n are the eigenvalues of $\hat{H}$, and the matrix,

$$\hat{Q}=\begin{pmatrix} \Delta t & -\dfrac{e^{-i\omega_{12}\Delta t}-1}{i\omega_{12}} & \cdots \\ \dfrac{e^{i\omega_{12}\Delta t}-1}{i\omega_{12}} & \Delta t & \cdots \\ \vdots & \vdots & \vdots \end{pmatrix} \tag{A16}$$

which is used to find the matrices of the integrated operators $\hat{\tilde{W}}^k$, $\hat{\tilde{U}}^k$, and $\hat{\tilde{Y}}^k$, see Eqs. (A7). The above operations are performed only once and before the actual propagation in time.

The leapfrog MD simulation gives the time-dependence of the QDS–bath coupling $\hat{W}$. Its matrix elements can be specified in any basis, but the transformation matrices to the diagonal basis of $\hat{H}$ have to be known. After setting up the QDS–bath couplings for the given time step, it is transformed to the diagonal basis of $\hat{H}$. Then, the matrix elements of integrated operators are found as

$$\begin{aligned} &\hat{\tilde{W}}^k_{lm}=\hat{Q}_{lm}\hat{W}_{lm}(q_k(t)), \quad \hat{\tilde{U}}^k_{lm}=ia_{lm}\hat{Q}_{lm}\hat{W}_{lm}(q_k(t)), \\ &\hat{\tilde{Y}}^k_{lm}=b_{lm}\hat{Q}_{lm}\hat{W}_{lm}(q_k(t)), \end{aligned} \tag{A17}$$

where there are *no summation* over indices, see also Eqs. (5), (6), (A4), and (A7).

At first time step of each MD trajectory the ''slipped'' initial conditions for the auxiliary matrix (8) are determined, which in the basis of eigenstates of $\hat{H}$ have the form

$$(\eta_{0k})_{lm}=b_{lm}\sum_j (\hat{W}_{lj}(q_k(0))\sigma_{0jm}+\sigma_{0lj}\hat{W}_{jm}(q_k(0))). \tag{A18}$$

Subsequently, we evaluate matrices $\hat{D}$, and $\hat{\Theta}^k(\sigma_0)$, see Eqs. (A10), (A11) and Eqs. (A12), (A13), respectively. The matrix elements of ξ are readily determined from Eqs. (A12), (A14), while the matrix elements of ϕ_k are found from Eq. (A9), using calculated values of ξ. When calculated ϕ_k we also added slow exponential decay to Eq. (A9) in order to compensate accumulation of errors at longer times.

The last operation required is to transform matrices ξ and ϕ_k back from the interaction representation to find $\sigma(\Delta t)$ and $\eta_k(\Delta t)$, correspondingly. It is readily done using a vector, defined by Eq. (A15), i.e.,

$$\begin{aligned} &\sigma_{lm}(\Delta t)=\mathbf{Z}^*_l\xi_{lm}(\Delta t)\mathbf{Z}_m, \\ &(\eta_k(\Delta t))_{lm}=\mathbf{Z}^*_l(\phi_k(\Delta t))_{lm}\mathbf{Z}_m, \end{aligned} \tag{A19}$$

where there is no summation over l,m, while asterisk denotes complex conjugate. The values of $\sigma(\Delta t)$ and $\eta_k(\Delta t)$ obtained in this way are used to calculate output values and replace the initial conditions $(\sigma_0,\ \eta_{0\,k})$ for the next step.

The suggested algorithm has relatively low computational cost and requires several matrix multiplications at each time step. The matrices involving exponentials (a_{lm}, b_{lm}, $\hat{Q}$, $\mathbf{Z}$), are calculated only once and stored before the propagation in time. This makes it possible to efficiently treat a multilevel systems with several hundred quantum states.

[1] W. G. Hoover, Annu. Rev. Phys. Chem. **34**, 103 (1983).
[2] D. J. Evans and G. P. Morriss, Comput. Phys. Rep. **1**, 297 (1984).
[3] F. G. Amar and B. J. Berne, J. Phys. Chem. **88**, 6720 (1984).
[4] Q. Liu, J.-K. Wang, and A. H. Zewail, J. Phys. Chem. **99**, 11321 (1995).
[5] S. Nose, J. Chem. Phys. **81**, 511 (1984).
[6] W. G. Hoover, Phys. Rev. A **31**, 1695 (1985).
[7] G. A. Voth, D. Chandler, and W. H. Miller, J. Phys. Chem. **91**, 7749 (1989); **93**, 7009 (1989).
[8] J. C. Tully, J. Chem. Phys. **93**, 1061 (1990).
[9] M. Topaler and N. Makri, Chem. Phys. Lett. **210**, 285 (1993).
[10] M. Morillo and R. I. Cukier, Phys. Rev. B **54**, 13962 (1997).
[11] I. A. Goychuk, E. G. Petrov, and V. May, Phys. Rev. E **56**, 1421 (1997).
[12] S. Nielsen, R. Kapral, and G. Ciccotti, J. Chem. Phys. **112**, 6543 (2000).
[13] G. Stock, J. Chem. Phys. **103**, 1561 (1995).
[14] A. Suárez, R. Silbey, and I. Oppenheim, J. Chem. Phys. **97**, 5101 (1992).
[15] R. B. Gerber, V. Buch, and M. A. Ratner, J. Chem. Phys. **77**, 3022 (1982).
[16] H.-D. Meyer and W. H. Miller, J. Chem. Phys. **70**, 3214 (1979).
[17] E. J. Heller, J. Chem. Phys. **62**, 1544 (1975); **75**, 2923 (1981).
[18] R. Car and M. Parrinello, Phys. Rev. Lett. **55**, 2471 (1985).
[19] A. G. Redfield, Adv. Magn. Reson. **1**, 1 (1965).
[20] K. Blum, *Density Matrix Theory and Applications* (Plenum, New York, 1981).
[21] C. P. Slichter, *Principles of Magnetic Resonance* (Springer, Berlin, 1990).
[22] W. T. Pollard and R. A. Friesner, J. Chem. Phys. **100**, 5054 (1994).
[23] C. Meier and D. J. Tannor, J. Chem. Phys. **111**, 3365 (1999).
[24] H.-P. Breuer, B. Kappler, and F. Petruccione, Phys. Rev. A **59**, 1633 (1999).
[25] T. Mančal and V. May, J. Chem. Phys. **114**, 1510 (2001).
[26] J. Wilkie, J. Chem. Phys. **114**, 7736 (2001).
[27] A. A. Neufeld, J. Chem. Phys. **119**, 2488 (2003), preceding paper.
[28] D. W. Oxtoby, Adv. Chem. Phys. **47**, 487 (1981).
[29] J. Chesnoy and G. M. Gale, Adv. Chem. Phys. **70**, 297 (1988).
[30] M. Tuckerman and B. J. Berne, J. Chem. Phys. **98**, 7301 (1993).
[31] J. C. Owrutsky, D. Raftery, and R. M. Hochstrasser, Annu. Rev. Phys. Chem. **45**, 519 (1994).
[32] S. A. Egorov and J. L. Skinner, J. Chem. Phys. **105**, 7047 (1996).
[33] P. Schofield, Phys. Rev. Lett. **4**, 39 (1960).
[34] P. A. Egelstaff, Adv. Phys. **11**, 203 (1962).
[35] P. Gaspard and M. Nagaoka, J. Chem. Phys. **111**, 5676 (1999).
[36] V. S. Vikhrenko, D. Schwarzer, and J. Schroeder, Phys. Chem. Chem. Phys. **3**, 1000 (2001).
[37] M. P. Allen and D. J. Tildesley, *Computer Simulation of Liquids* (Clarendon, Oxford, 1996).
[38] D. Rostkier-Edelstein, P. Graf, and A. Nitzan, J. Chem. Phys. **107**, 10470 (1997).
[39] G. Käb, Phys. Rev. E **66**, 046117 (2002).